electronics

MDPI

Article

An Active and Passive Hybrid Battery Equalization Strategy Used in Group and between Groups

Mingyu Gao [1,2], Jifeng Qu [1,2], Hao Lan [1,2], Qixing Wu [1,2,3], Huipin Lin [1,2,*], Zhekang Dong [1,2] and Weizhong Zhang [3]

1 College of Electronic Information, Hangzhou Dianzi University, Hangzhou 310018, China; mackgao@hdu.edu.cn (M.G.); qujifeng@hdu.edu.cn (J.Q.); lh123456@hdu.edu.cn (H.L.); wuqixing@zime.edu.cn (Q.W.); englishp@hdu.edu.cn (Z.D.)
2 Zhejiang Provincial Key Lab of Equipment Electronics, Hangzhou Dianzi University, Hangzhou 310018, China
3 Faculty of Automation, Zhejiang Institute of Mechanical and Electrical Engineering, Hangzhou 310018, Zhejiang, China; zhangweizhong@zime.edu.cn
* Correspondence: linhuipin@hdu.edu.cn

Received: 2 September 2020; Accepted: 19 October 2020; Published: 21 October 2020

Abstract: Active battery equalization and passive battery equalization are two important methods which can solve the inconsistency of battery cells in lithium battery groups. In this paper, a new hybrid battery equalization strategy combinfigureing the active equalizing method with a passive equalizing method is proposed. Among them, the implementation of the active equalizing method uses the bidirectional Flyback converter and Forward converter. This hybrid equalizing strategy adopts the concept of hierarchical equilibrium: it can be divided into two layers, the top layer is the equalization between groups, and the bottom layer is the equalization of group. There are three active equilibrium strategies and one passive equilibrium strategy. For verification purposes, a series of experiments were conducted in MATLAB 2018b/Simulink platform. The simulation and experiment results show that this hybrid battery equalizing method is efficient and feasible.

Keywords: hybrid battery equalization; Li-ion battery; passive equalization; active equalization; bidirectional flyback converter; bidirectional forward converter

1. Introduction

The advantages of a lithium-ion battery are its high-energy density, low self-discharge rate, cycling durability, and wide temperature range [1]. Due to its excellent performance, lithium-ion battery has become the best choice for electric vehicles and other energy storage systems. Due to the differences in the manufacturing and operating environment, inconsistency between the different batteries in the same battery group is existed [2]. The inconsistency brings about a loss of capacity of the battery group, and it eventually leads to shorter battery life. A statistic shows that the capacity difference in different batteries of the same model can reach 20% [3], bcause the capacity loss of one battery group can reach 40%. As time goes on, the inconsistency of batteries will increase. Battery equalizing is an effective way to reduce the battery decay rate in battery management systems (BMSs). Battery equalizing mainly focuses on the investigation of equalization topology and control algorithms [4–6].

The battery equalizing technology plays a vital role in the performance improvement for lithium-ion batteries. Nowadays, there are two main battery-balancing methods: passive equalizing and active equalizing [7–10]. The passive equalizing method is that the energy of higher-power batteries is dissipated by one simple resistive circuit, and the energy is wasted in passive equalizing [11–14]. Active equalizing mainly realizes the non-dissipative transfer of energy in the battery group through energy storage components. The main active equalization methods are shown in Figure 1 [1]. In traditional

active equalization, the topology usually adopts a single equalization method. One active equalizing method that one cell transfers energy to adjacent cells step by step, thus the equalizing speed is very slow. Another active equalizing method is that the energy is transferred between the battery cell and the battery group [15–18]. However, it has a disadvantage of repeated energy transfer. All of these active equalizing methods have significant limitations in their equalization speed and equalization efficiency. The equalization topology regularly adopts the Flyback converter or the Forward converter [19]. In these two topologies, a large amount of MOSFETs swiches are turned on or off at the same time, which may increase cost and reduce reliability. It is evident that using a single active or passive equalizing topology cannot meet actual needs [20,21]. For these reasons, a hybrid equalization topology is proposed in this paper. By combining multi-layer active equalization with passive equalization, the energy equalization of the battery group can be realized in different situations. The paper mainly includes the principle of the hybrid equalization topology, equalization efficiency analysis/calculation, experimental verification and conclusion [22].

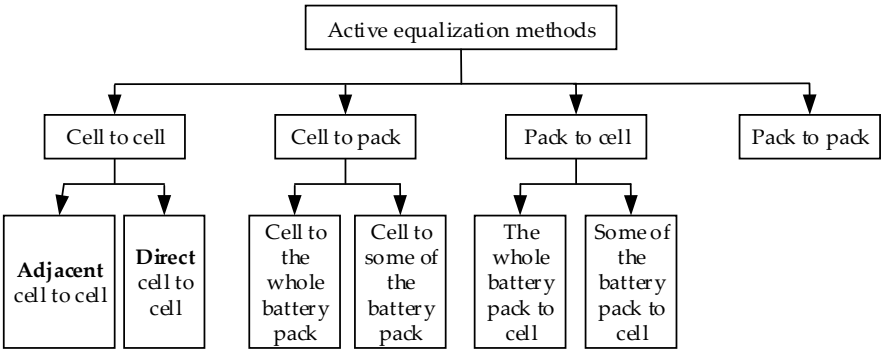

Figure 1. Classification of active equalization methods.

Figure 2 shows the system architecture of the proposed battery equalization topology. The topology contains the bidirectional forward and bidirectional flyback converters. The structure can be divided into two layers, the top layer is the between-group equalization, and the bottom layer is the in-group equalization. There are m × n battery cells in the system, each n cells forming one battery group, with m groups in total. So, the sub-circuits between the battery groups constitute the between-group equalization system, and the sub-circuits internal to the battery group form the between-group equalization system.

The in-group equalization system is composed of active and passive equalization. The active equalization sub-circuit consists of two reverse-series MOSFETs, a winding of the transformer, an auxiliary MOSFET, and a capacitor. The equalization sub-circuits of different batteries are connected by a multi-winding transformer. The turns ratio of the transformer is 1:1:1:1. The MOSFET interconnected to the battery can replace the diode of the traditional Flyback converter or the Forward converter. In addition, the conduction loss of the MOSFET is much less than that of the diode in the traditional converter topology. The passive equalization sub-circuit of each battery includes a MOSFET and a dissipative resistor. The energy of the higher-capacity cell can be released through the dissipative resistor by changing the switching states of the MOSFET.

The between-group equalization is adopted on the bi-drectional Flyback converter. Each battery group in this layer can charge to any battery cell with higher voltage and larger capacity, and the Flyback converter and the battery group are connected one to one. The primary side of the equalizer is the corresponding battery group, and the secondary side is the entire power supply system. The between-group equalization can realize bidirectional energy flow between the battery group and the entire power supply system.

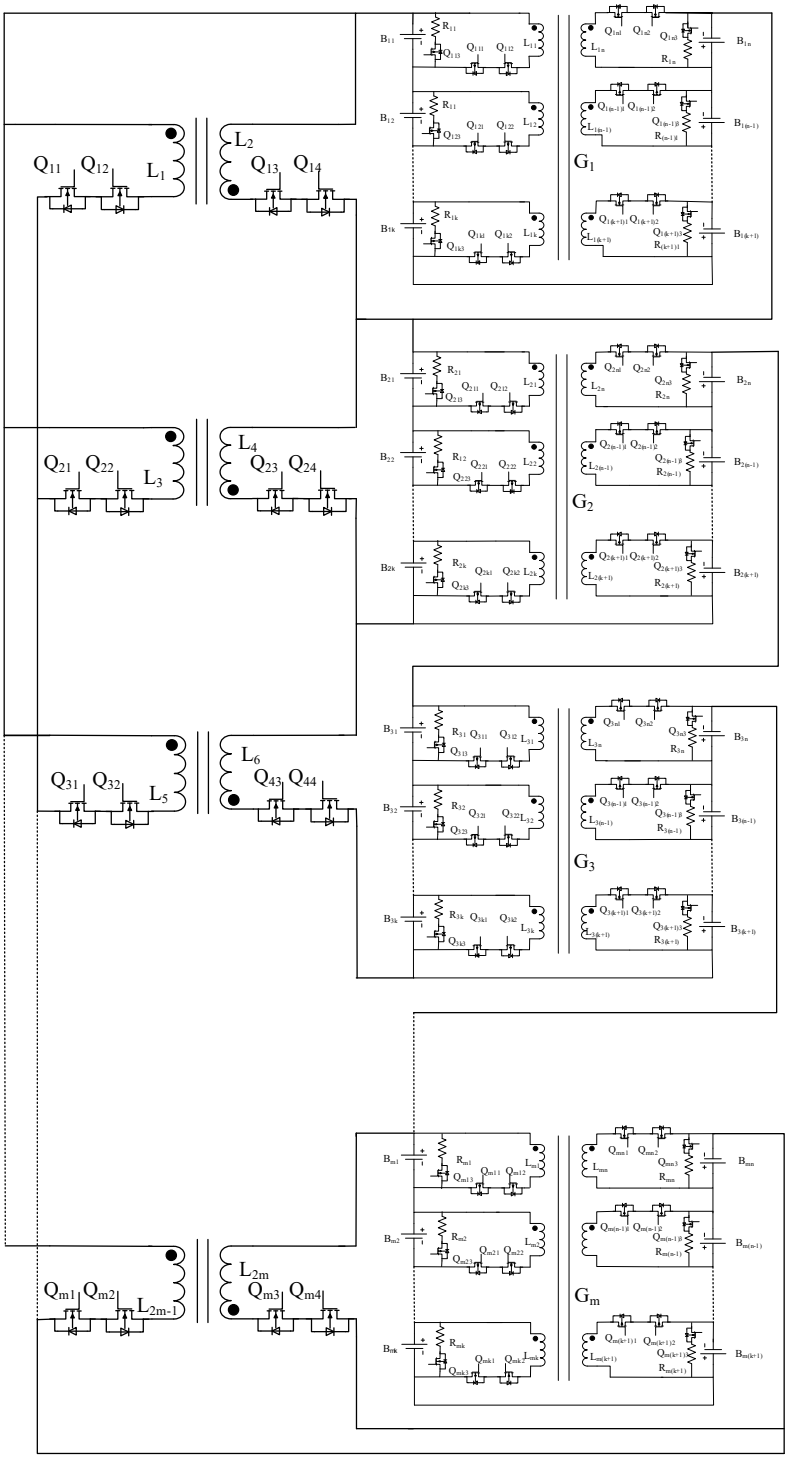

Figure 2. Overall battery equalization circuit topology.

This topology is a double-layer hybrid topology. It adopts an equalization strategy which combines active and passive balancing to improve the balancing efficiency. In addition, because of the double-layer design, it can be used in scenarios where the number of cells is large, and different layers can be balanced at the same time, which significantly reduces the time required for equalization. The bidirectional flyback converter can complete the energy equalization at a higher power level. The active equalization sub-circuit in each group can flexibly realize the energy exchange between cells. Besides, it is supplemented by a passive equalization circuit. The passive equalization method

was used as when the voltage difference between battery cells is small, it can accelerate equalization. Specifically, there are four equalization modes (containing three in-group equalization modes and one between-group equalization circuit mode). The corresponding mode description is introduced below.

In the schematic diagram of in-group equalization in each group, taking four cells as an example, the cells are divided into two sides, B_{11} and B_{12} are on the left side, and B_{13} and B_{14} are on the right side. According to the position where the target battery and the source battery are located, the battery balancing topology proposed in this paper contains three in-group balancing modes and one between-group balancing mode.

1.1. MODE 1: In-Group Flyback Mode

If the target battery and the source battery are on different sides of the battery group, the energy is transferred between the batteries by the Flyback operation. Assuming that B_{11} is the source battery and B_{13} is the target battery, at time t_1, Q_{111} and Q_{112} are turned on, Q_{113} and all other MOSFETs are turned off. The energy is transferred from battery B_{11} to transformer L_{11} for storage. In $[t_1, t_2]$, the discharge current is calculated as Equation (1), and the current flow direction is shown in Figure 3a. At time t_2, Q_{111}, Q_{112} and Q_{113} are turned off; Q_{131} and Q_{132} are turned on. Most of the energy in L_{11} is released to the Battery B_{13}. At this time, the current flowing through the inductor L_{13} is located and can be calculated according to the superposition theorem, in Equation (3), $i_{B13}(t_2)$ represents the initial value of the current at time t_2, the relationship between $i_{B13}(t_2)$ and the current value $i_{B11}(t_2)$ of the primary winding at time t_2 is shown in Equation (2). The voltage across the winding L_{13} is clamped to voltage V_{B13} by the battery cell, so $i_{B13}(t)$ gradually decreases with time, Equation (3) expresses this decay process. Due to the leakage inductance of L_{11}, the current cannot be entirely transferred to the other side when Q_{111} and Q_{112} are turned off. At the time of $[t_2, t_3]$, the charge current of B_{13} is calculated as Equation (3). Eventually, the energy is transferred from B_{11} to B_{12}. The MOSFET switching state of the whole process is shown in Figure 4a:

$$i_{B_{11}}(t) = \frac{V_{B_{11}}}{L_{11}}(t - t_1) \tag{1}$$

$$i_{B_{13}}(t_2) = i_{B_{11}}(t_2) \tag{2}$$

$$i_{B_{13}}(t) = i_{B_{13}}(t_2) - \frac{V_{B_{13}}}{L_{13}}(t - t_2) \tag{3}$$

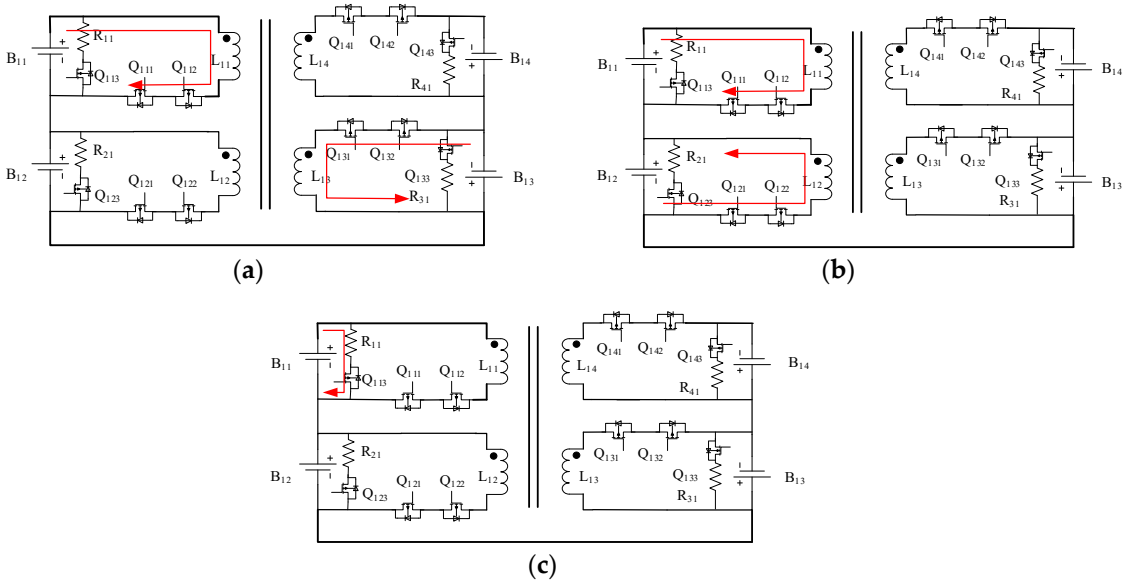

Figure 3. Three in-group-pack equalization circuit modes: (**a**) MODE 1; (**b**) MODE 2; and (**c**) MODE 3.

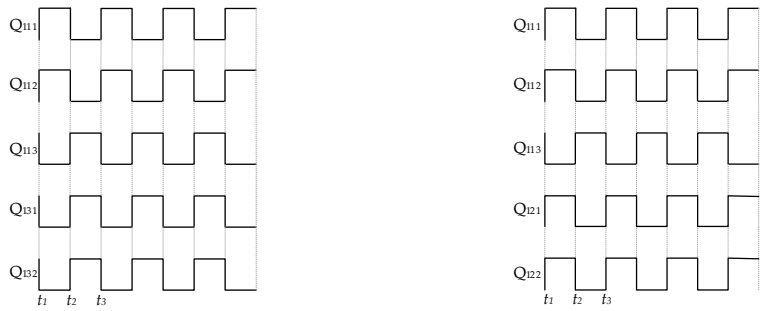

Figure 4. Control signal: (**a**) MODE 1; and (**b**) MODE 2.

1.2. MODE 2: In-Group Forward Mode

If the target battery and the source battery are on the same side and the voltage difference is larger than 150 mV, the energy is transferred between batteries by the forward operation. We assumed that B_{11} is the source cell and B_{12} is the target cell. At time t_1, Q_{111}, Q_{112}, Q_{121}, and Q_{122} are all turned on, and the energy of the cell B_{11} is directly transmitted to B_{12} through the transformer. At time [t_1, t_2], the current is calculated as Equation (4), and the current flow direction is shown in Figure 3b. At the time t_2, the switches Q_{111}, Q_{112}, Q_{121}, and Q_{122} are turned off, the energy transfer is finished. In the [t_1, t_2], the maximum current value can be calculated as Equation (4). The R represents the equivalent impedance of the entire loop:

$$I_{loop} = \frac{V_{B_{11}} - V_{B_{12}}}{R} \tag{4}$$

Finally, the energy transformation from the source battery to the target battery is realized, and the MOSFET control signal for the entire process is shown in Figure 4b.

1.3. MODE 3: In-Group Passive Balancing Mode

If the target battery and the source battery are in the same group, and the batteries do not satisfy the condition that the voltage difference is large enough, active equalization is not suitable. In this case, the topology adopts the passive equalization, which is very suitable for the equalization with the batteries with small inconsistencies. Take B_{11} as an example: Q_{113} is turned on and other MOSFETs are turned off. As shown in Figure 3c. At this time, the on-resistance of the MOSFET is ignored, and the current can be calculated according to (4). The passive equalization of other battery cells is the same as the above process. Eventually, the excess energy is dissipated in the form of heat:

$$i_{B_{11}}(t) = \frac{V_{B_{11}}}{R_{11}} \tag{5}$$

1.4. MODE 4: Between-Group Bidirectional Flyback Mode

If there is a difference between the battery groups, the topology adopts a between-group mode. The triggering condition of the mode is the maximum voltage difference larger than 80 mV. The bidirectional flyback active balancing circuit transfers energy from the higher-power battery group to the entire power supply system by controlling the switch of the MOSFET, or vice versa. This paper uses the balancing between two battery groups as an example to explain the working principle of the between-group balancing. As shown in Figure 5a, assuming that the battery group where B_{11} is in higher energy state, the battery group where B_{11} is located serves as the primary side of the Flyback transformer, and the power supply system serves as the secondary side of the Flyback converter. Q_{13}, Q_{14}, and Q_{11}, Q_{12} are turned on or off by complementary pulse-width modulation (PWM) driving signals, respectively. At this time, the battery group charges the whole power supply system through the flyback converter. The current flow is shown in Figure 5a: the converter works in DCM mode,

the duty cycle is set to 45%, and according to the transformer transformation ratio it is 1:m, with m being number of bottom groups, where m = 2 when Q_{13} and Q_{14} are turned on, battery pack G_1 charges winding L_2, V_{g1} is the voltage value of G_1. The peak value of the primary charging current I_{pri_pk} is calculated according to Equation (6). Then, the average current value I_{pri_aver} is obtained by Equation (7). After that, Q_{13} and Q_{14} are turned off, and Q_{11} and Q_{12} are turned on. At this time, the secondary winding discharges to the entire top layer group, and the initial value of the secondary current is its peak value. Its value is represented by Equation (8), and the average value of the secondary winding current is represented by Equation (9):

$$I_{pri\_pk} = \frac{V_{g1} T_{on}}{L_2} \tag{6}$$

$$L_{pri\_aver} = \frac{1}{2} T_{on} I_{pri\_pk} = \frac{V_{g1} T_{on}^2}{2L_2} \tag{7}$$

$$I_{sec\_pk} = \frac{1}{2} I_{pri\_pk} \tag{8}$$

$$I_{sec\_aver} = \frac{1}{2} T_{off} I_{sec\_pk} = \frac{1}{2} T_{off} * \frac{1}{2} I_{pri\_pk} = \frac{V_{g1} T_{on} T_{off}}{4L_2} \tag{9}$$

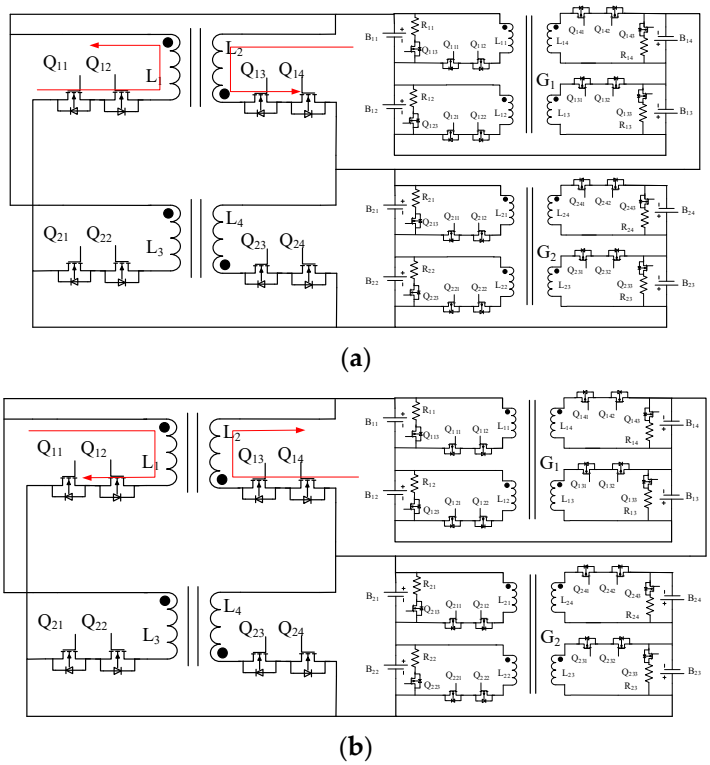

Figure 5. Schematic diagram of the bidirectional flyback converter in inter-pack, (**a**) Energy transfers from the group G_1 to the top layer group, (**b**) Energy transfers from the top layer group to group G_1.

In another case, when the energy of the battery group in the entire power supply system is lower than the average level, by controlling the corresponding MOSFET to be turned on and off, the energy of the entire power supply system can be transferred to the lower power battery group. Assuming that the power level of B_{11} at this time is lower than the average level, the bidirectional flyback converter is configured as a buck converter to charge it. At this time, L_1 in Figure 5a is the primary-side transformer winding, and (Q_{13},Q_{14}), (Q_{11},Q_{12}) are turned on or off by the complementary PWM drive, respectively. The whole power supply sysem is charged to the battery group with a lower energy level, and the

current flow is shown in Figure 5b, that when Q_{11} and Q_{12} are turned on, L_1 is charged, V_{total} is the voltage of the top battery group, and its expression is Equation (11). At this time, the top group side is the primary side of the transformer, the peak charging current of the primary side is calculated according to Equation (12). Then, the average current value is obtained by Equation (13). After Q_{11}, Q_{12} are turned off, Q_{13}, Q_{14} are turned on, the secondary winding discharges to the battery group G_1. The initial value of the secondary current at this time is the peak value, which is expressed by Equation (14), and the average current value is expressed by Equation (15).

$$I_{pri\_pk} = \frac{V_{total} T_{on}}{L_1} \tag{10}$$

$$V_{total} = V_{g1} + V_{g2} \tag{11}$$

$$I_{pri\_pk} = \frac{(V_{g1} + V_{g2}) T_{on}}{L_1} \tag{12}$$

$$I_{pri\_aver} = \frac{1}{2} T_{on} I_{pri\_pk} = (\frac{V_{g1} + V_{g2}}{2L_1}) T_{on}^2 \tag{13}$$

$$I_{sec\_pk} = 2 I_{pri\_pk} \tag{14}$$

$$I_{sec\_aver} = \frac{1}{2} T_{off} I_{sec\_pk} = \frac{V_{total} T_{off} T_{on}}{L_1} = (\frac{V_{g1} + V_{g2}}{L_1}) T_{off} T_{on} \tag{15}$$

2. Performance Evaluation

In order to evaluate the balancing performance of the proposed topology, we compared the proposed topology and the adjacent batteries balancing topology (as shown in Figure 6) [17] (position). In the rest of this section, we specifically analyze the equalization efficiency. We assume that there are n cells in the battery group, and the equalization efficiency of each sub-equalizer is η.

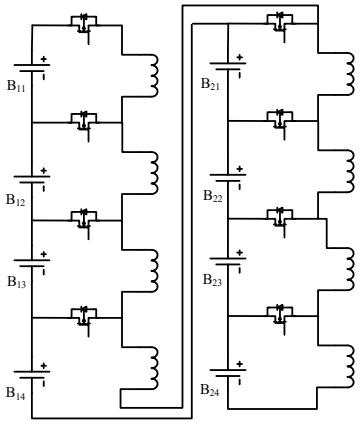

Figure 6. The adjacent batteries' balancing topology.

2.1. The Adjacent Batteries Balancing Topology

In the adjacent batteries' balancing topology, there are $n - 1$ kinds of unbalanced state (x_1, x_2, x_3, ... , x_{n-1}), corresponding to the $n - 1$ balancing efficiency (η^1, η^2, η^3, ... , η^{n-1}). The distribution of the balancing efficiency is shown in Figure 6. Assuming that the state of charge (SOC) of the cells in the battery group is arbitrary, there is a total of $n \cdot (n - 1)$ balancing states, and the average balancing efficiency of the entire system depends on the current unbalanced state of the system. Assuming that the balancing efficiency value $\eta(\mathrm{i})$ is determined by the given unbalance state x_i. The probability

of $(x = x_i)$ is calculated as Equation (16). The expected value of the balancing effect of the adjacent batteries' balancing topology is calculated as Equation (17):

$$P(x = x_i) = \frac{2(n-i)}{n(n-r)} \tag{16}$$

$$\begin{aligned} E(\eta) &= \sum_{i=1}^{n-1} \eta(i) P(x = x_i) = \sum_{i=1}^{n-1} \eta^i \frac{2(n-i)}{n(n-1)} \\ &= \frac{2\eta(1-\eta)\left(1-\eta^{n-1}\right)(n-1)+\eta^{n-1}(1-\eta)(2n-3)-\eta\left(1-\eta^{n-1}\right)}{(n-1)(2n-3)(1-\eta)^2} \end{aligned} \tag{17}$$

2.2. The Proposed Topology

For the topology proposed in this paper, the efficiency of the balancing between the battery cells is assumed to be η. Then, there is only active balancing in the in-group balancing, and the efficiency is η. Therefore, the expected balancing efficiency of the proposed topology is calculated as Equation (18):

$$E(\eta) = \sum_{i=1}^{n-1} x_i P(x = x_i) = \eta \tag{18}$$

Once the equalization circuit is built up, the efficiency η is a constant. This paper assumes $\eta = 0.9$. The expectation curve is shown in Figure 7. The blue curve is the adjacent batteries' balancing topology, and the orange curve is the topology proposed in this paper. If $n < 3$, the adjacent cells' balancing topology is more efficient. If $n = 3$, the efficiency of the two topologies is approximately equal. However, if $n > 3$, the efficiency of the proposed topology in this paper is obviously higher. As the number of batteries increases, the topology performance proposed in this paper is more obvious. Since lithium battery groups usually have a large number of batteries in series under actual conditions, the topology proposed in this paper has great advantages in performance. According to the above analysis, the proposed topology can directly transmit energy and the adjacent batteries' balancing topology can only be transmitted between the adjacent batteries, so it can be seen that the topology of this paper has a faster speed. Tables 1 and 2 show the performance comparison between the solution proposed in this paper and other common solutions.

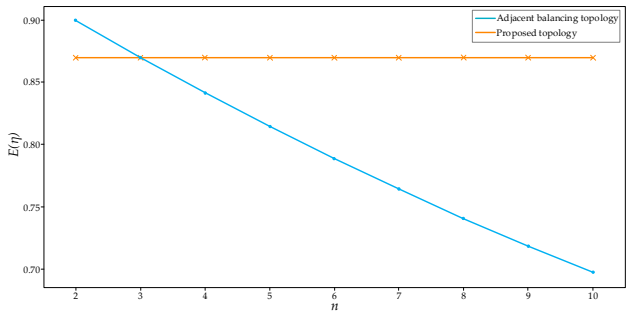

Figure 7. The efficiency curve.

Table 1. Component quantity comparison.

Method	Switch	Resistor	Capacitor	Inductor	Transformer	Diode
Single-trans.	2n + 1	-	-	-	1	1
Multi-trans.	2n	-	-	-	n	n
Multi-layer	2n + 4m	-	-	-	n + m	-
Capacitor	2n	-	n − 1	-	-	-
Inductor	4n	-	-	1	-	4n
Passive	n	n	-	-	-	-
Proposed method	3n + 4m	n	-	-	2m	-

Table 2. Perfomence comparsion.

Method	Speed	Efficiency	Condition	Complexity	Cost	Suitable String
Single-trans.	Medium	Medium	Ch/disch	Complex	Medium	Medium
Multi-trans.	Medium	High	Ch/disch	Simple	Medium	Long
Multi-layer	Quick	Medium	Ch/disch	Medium	High	Very long
Capacitor	Very slow	Very high	Ch/disch	Simple	Low	Medium
Inductor	Quick	Very high	Ch/disch	Simple	low	Medium
Passive	Very slow	-	Charge	Very simple	Very Low	Long
Proposed method	Very quick	Very high	Ch/disch	Medium	Medium	Very long

3. Simulation

MATLAB 2018b/Simulink was used to validate the topology proposed in this paper. This paper will verify the in-group and between-group balancing separately.

The intra-in-group balancing circuit was built by the components in the Simscape library in Simulink. The battery model parameters used in the simulation are used the parameters of ternary lithium battery, they are set as shown in Table 3. The circuit is shown in Figure 8, PWM_G1_1, PWM_G1_2, PWM_G1_3, and PWM_G1_4 are the driving signals of the bidirectional switch respectively, and each signal is a 100 kHz PWM waveform, Each bidirectional switch applies different drive waveforms according to different working modes, When the circuit works in the flyback equilibrium mode, the phase difference of the switching drive waveforms of the two cells for energy transfer is 180°, When in the forward equilibrium mode, the switching drive waveforms of the two cells for energy transfer are the same in phase. PASSIVE_G1, PASSIVE_G2, PASSIVE_G3, PASSIVE_G4 are control switches for passive equalization discharge resistance respectively, The switch is opened when operating the cell that needs to be discharged.

Table 3. The battery model parameters for simulation.

Battery Model Type	Lithium-Ion
Nom-Voltage	3.7 V
Rated capacity	2.8 Ah
Internal resistance	30 mΩ
Nom-voltage capacity	2.3 Ah
Fully charged voltage	4.1 V

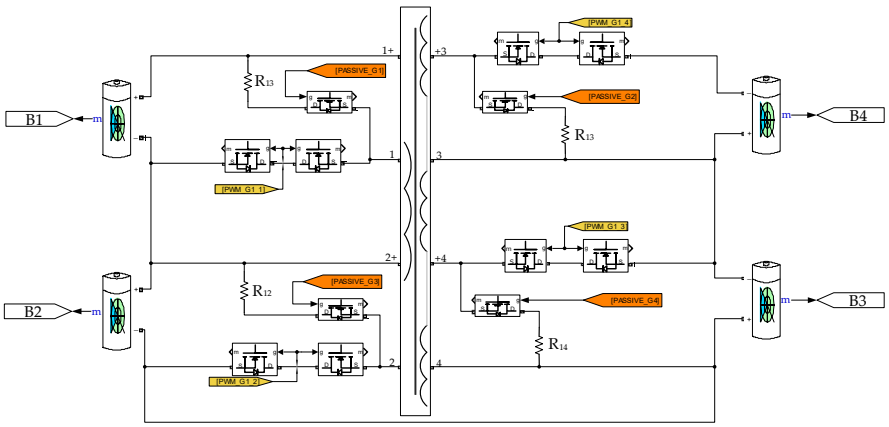

Figure 8. The simulation circuit diagram of in-group equalization.

(1) In the simulation, MODE 1 is first verified. The condition that the balanced topology works in MODE 1 is that the highest and lowest battery cells are on different sides of the battery group. *B*1 is the source battery in the balancing process, and *B*3 is the target battery. The initial SOCs of *B*1 and *B*3 are

set to 99% and 30%, respectively. At this time, the gate drive waveforms of the corresponding MOSFET in the balancing circuits of $B1$ and $B3$ were shown in Figure 9. It can be seen that the phase difference between the two was 180°, so the PWM signals were complementary. The circuit worked in the in-group Flyback Mode. The current and voltage waveforms on the bidirectional switch are shown in Figure 10: the working frequency was 100 kHz, the rated output power was set to 4.5 W, the efficiency was set to 85%, the duty cycle was set to 45%, the calculation process of the primary magnetizing inductance and leakage inductance were as processed in Equation (19), the transformer leakage inductance was estimated to be 5% of the magnetizing inductance, and the copper loss resistance of the primary winding was set to 25 m·Ω.

$$\begin{aligned} P_{in} &= \frac{P_o}{\eta} = \frac{4.5\ W}{0.85} \approx 5.3\ W \\ I_{aver} &= \frac{P_{in}}{V_{\min}} = \frac{5.3\ W}{3.7\ V} \approx 1.43\ A \\ I_{pri\_pk} &= \frac{I_{aver}}{0.5\ D} = \frac{1.43\ A}{0.5{*}0.45} \approx 6.36\ A \\ L_{pri} &= \frac{V_{in} T_{on}}{I_{pk}} = \frac{3.7\ V{*}10\ \mu s{*}0.45}{6.36\ A} \approx 2.62\ \mu H \\ L_{leakage} &= L_{pri} * 0.05 = 2.62\ \mu H * 0.05 \approx 0.131\ \mu H \end{aligned} \tag{19}$$

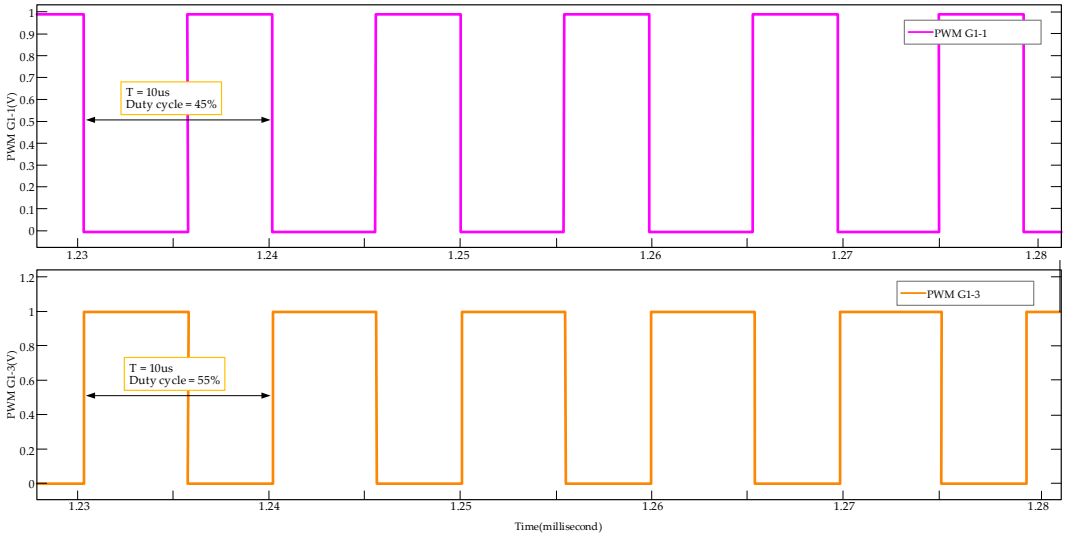

Figure 9. The waveform of PWM_G1_1 and PWM_G1_3 in MODE 1.

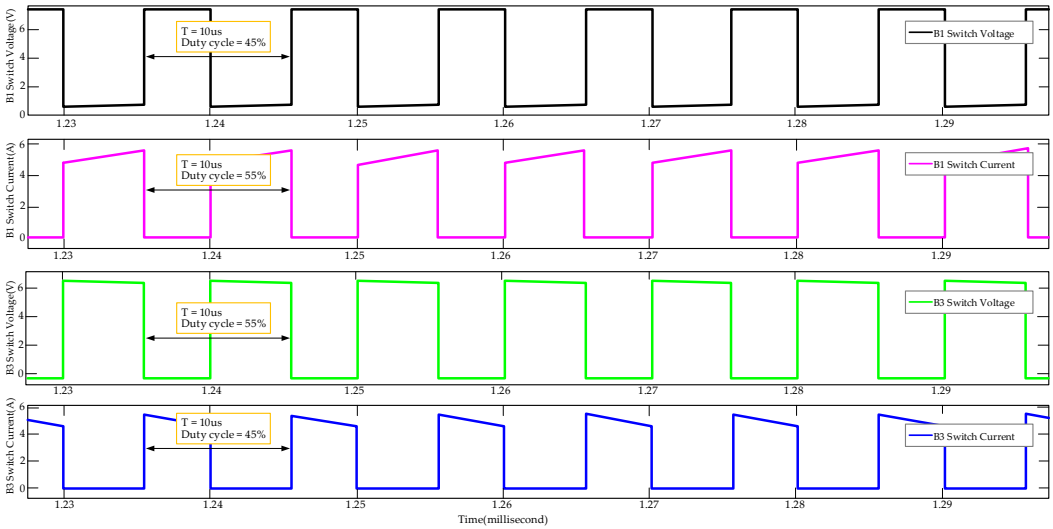

Figure 10. The current and voltage waveform of MODE 1.

According to the simulation results in Figure 11, it is clear that the equilibrium time is 731.7 s. By Equation (20), the balancing efficiency of this equalization is about 82.1%. The simulation results show that the topology proposed in this paper can realize the balancing mode of MODE 1, and the balancing efficiency and equalization speed meet the expectation:

$$P = \frac{SOC_{B1\_end} + SOC_{B3\_end}}{SOC_{B1\_before} + SOC_{B3\_before}} \tag{20}$$

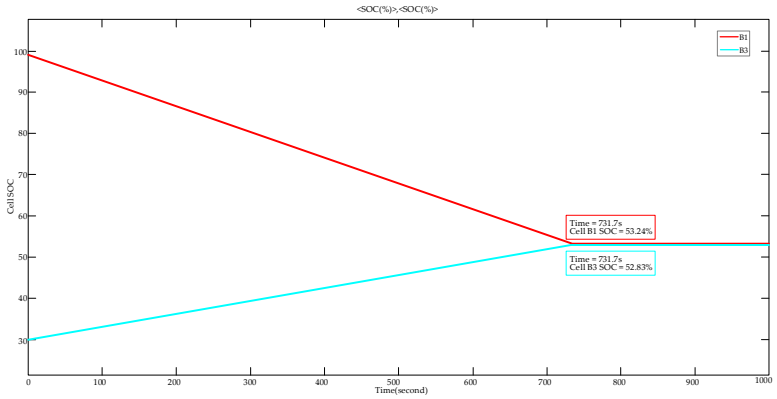

Figure 11. The state of charge (SOC) curve during balancing in MODE 1.

(2) In order to verify the MODE 2, $B1$ was chosen as the source battery, and $B2$ as the target battery. $B1$ and $B2$ are in the same side of the battery group. The initial SOC of $B1$ was set to 99%, and the initial SOC of $B2$ was set to 30%. At this time, the gate drive waveforms of the corresponding MOSFET in the balancing circuits of $B1$ and $B2$ are shown in Figure 12. It can be seen that the phase difference between the two is 0°, so that they are in-phase PWMs. The circuit works in the In-groupForward Mode. The current and voltage waveforms on the bidirectional switch at this time are shown in Figure 13. MODE 2 requires that the battery voltage difference exceeds the threshold, so at this time, the equalization time is completed at 1006.3 s by Figure 14. After balancing, the SOCs of $B1$ and $B2$ are 61.45% and 61.67%, respectively. Compared with the in-group flyback mode, it takes a longer time. The balancing efficiency of this calculation is 95.4% according to Equation (21):

$$P = \frac{SOC_{B1\_end} + SOC_{B2\_end}}{SOC_{B1\_before} + SOC_{B2\_before}} \tag{21}$$

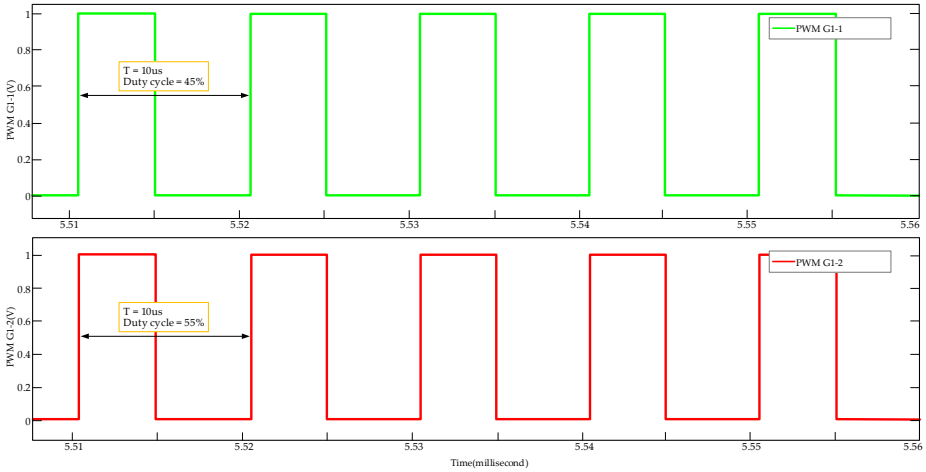

Figure 12. The driver waveform of PWM_G1_1 and PWM_G1_2 in MODE 2.

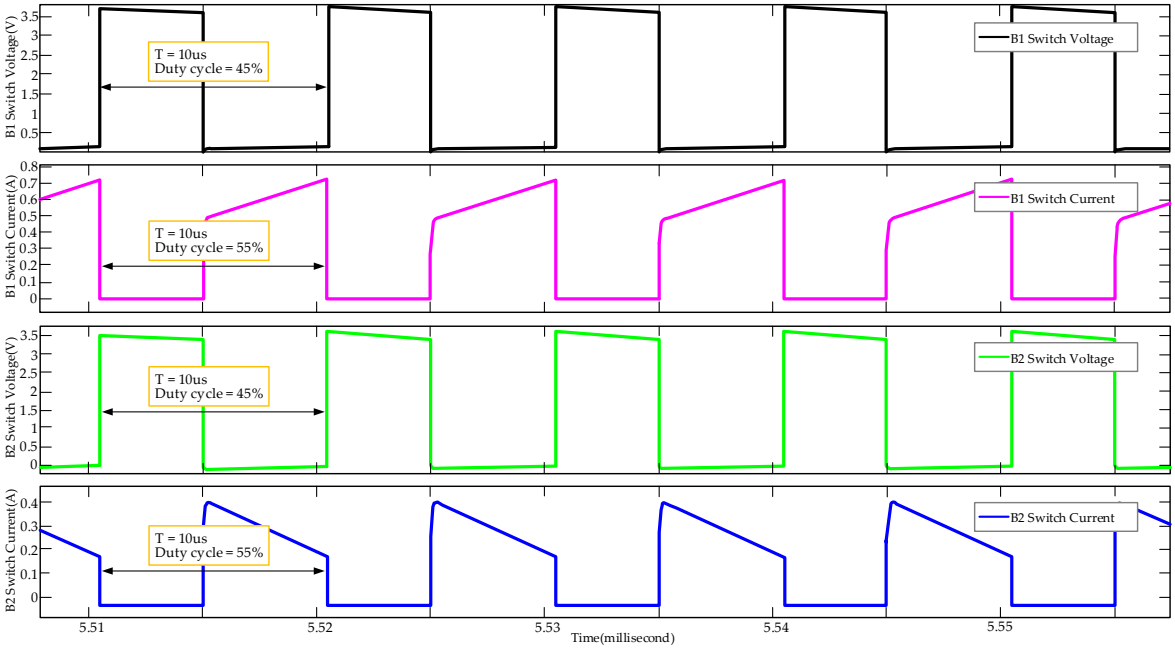

Figure 13. The current and voltage waveform of MODE 2.

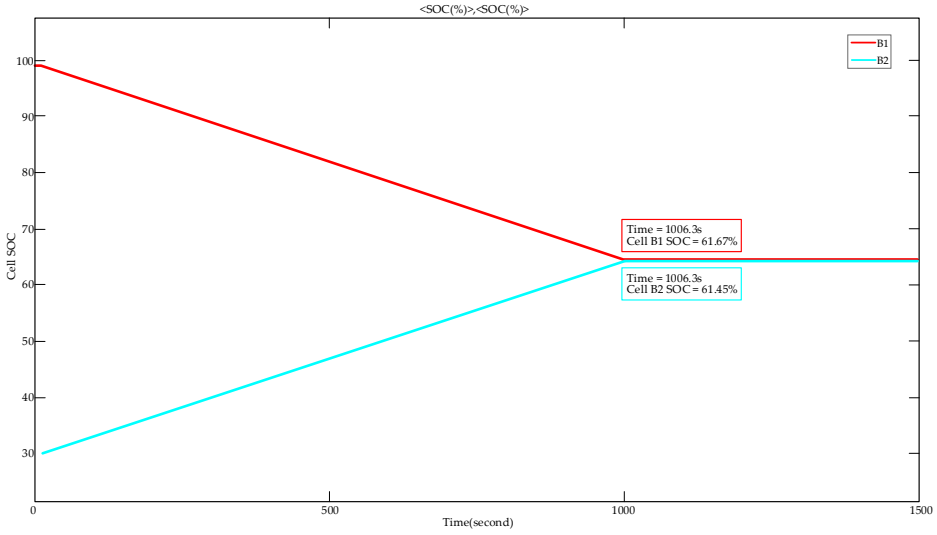

Figure 14. The SOC curve during balancing in MODE 2.

(3) This paper then verified MODE 3, in the in-group passive balancing mode. This mode requires that the SOC difference between the battery cells is less than 150 mV. The SOCs of four batteries are set to 80.4%, 80.2%, 80%, and 78.2%, respectively. At this time, the corresponding battery voltages are 3.465, 3.463, 3.459, and 3.443 V, and the maximum voltage difference is 22 mV, which exceeds the threshold of passive equalization. The SOCs at the final termination are 78.19%, 78.21%, 78.23%, and 78.18%, respectively. The entire balancing process takes 531.3 s. The SOC change curve in the process is shown in Figure 15.

(4) MODE 4 is the between-group bidirectional flyback mode. In Figure 16, taking the power supply system composed of four battery groups as an example, the energy exchange between the entire power supply system and one of the battery groups is used to achieve a balanced effect.

The between-group balancing should wait until the end of in-group balancing. Each battery group in the power supply system is equivalent to a large-capacity battery cell. Because the battery group is connected in series, the capacity of the equivalent battery group is equal to the sum of the capacities of

all the batteries in it, and the voltage of an equivalent battery group is equal to the sum of the voltage of all the series batteries in it. G_1, G_2, G_3, and G_4 are used to represent four battery groups in the power supply system, each of which has a rated voltage of 13.2 V.

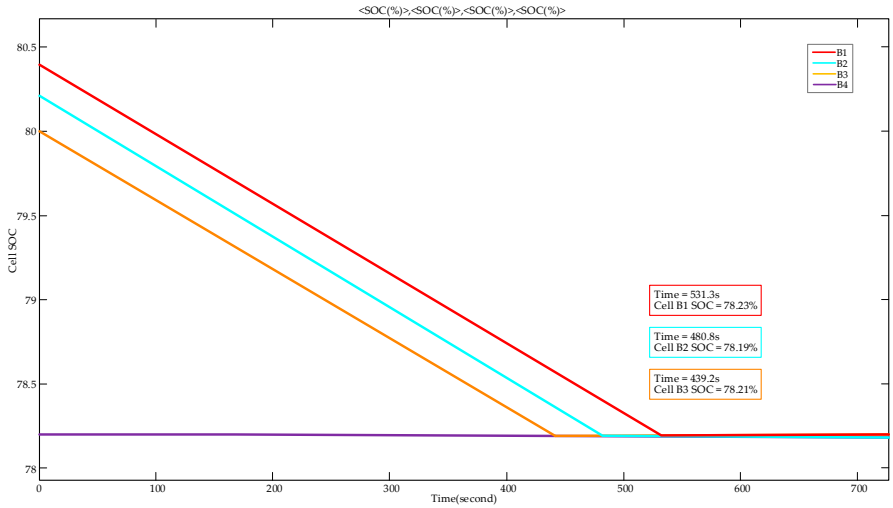

Figure 15. The SOC curve during balancing in MODE 3.

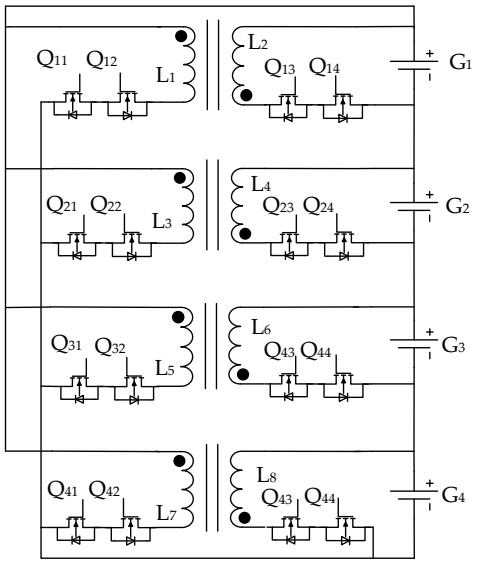

Figure 16. Bidirectional flyback topology for the between-group equalization.

The between-group balancing proposed in this paper adopts different control strategies for two different situations. First, the average voltage value of the four battery groups is obtained, and the number of battery groups that are lower than the average value and higher than the average value are obtained through comparison. If the number of battery groups higher than the average value is greater, the entire power supply system is used to charge the battery groups that are lower than the average value. On the other hand, a higher-voltage battery group is used to charge the entire power supply system to achieve balance. The termination conditions of the two equalization methods are set such that the absolute value of the difference between the voltage values of all battery groups and the average voltage of the entire power supply system is less than 180 mV. The top-level active equalization simulation is carried out using the circuit diagram shown in Figure 8, which only needs to reasonably set and modify the voltage of the battery, and one bottom-layer group is composed of four cells, its nominal voltage being $V_{g\_nom} = 3.7\ V$. The nominal voltage of the entire top layer group is

$V_{total} = 4V_{g\_nom} = 59.2\ V$, the top group side is defined as the primary side, the turn ratio is set to 4:1, the output power of the flyback converter between groups is set to 40 W. The efficiency is calculated at 85%, the switching frequency is set to 100 kHz, the leakage inductance of the primary winding is estimated as 5% of the magnetizing inductance, the calculation process of the transformer parameters are expressed as Equation (22). The following will verify this mode:

$$\begin{aligned} P_{in} &= \frac{P_o}{\eta} = \frac{40\ W}{0.85} \approx 47\ W \\ I_{aver} &= \frac{P_{in}}{V_{\min}} = \frac{47\ W}{59.2\ V} \approx 0.8\ A \\ I_{pri\_pk} &= \frac{I_{aver}}{0.5\ D} = \frac{0.8\ A}{0.5 * 0.45} \approx 3.6\ A \\ L_{pri} &= \frac{V_{in} T_{on}}{I_{pk}} = \frac{59.2\ V * 10\ \mu s * 0.45}{3.6\ A} \approx 74\ \mu H \\ L_{leakage} &= L_{pri} * 0.05 = 74\ \mu H * 0.05 \approx 3.7\ \mu H \end{aligned} \tag{22}$$

(a) CASE 1: The entire power supply system charges a single battery group.

Considering the practical application, the experiment uses the voltage of the battery group as the variable of the between-group balancing. The initial voltages of G_1, G_2, G_3 and G_4 are set to 14.345 V, 14.320 V, 13.961 V and 14.292 V, respectively. At this time, the average voltage of the entire power supply system is 14.230 V, and an equalization strategy for charging the battery group G_3 by the entire power supply system should be adopted.

At this time, Q_{31}, Q_{32}, Q_{43}, and Q_{44}, shown in Figure 17, are controlled by two complementary PWMs, respectively, and the circuit with the same structure as Q_{31} and Q_{32} is hereinafter referred to as a bidirectional switch. The turns ratio of the transformer is selected as 4:1. Since the secondary group is charged for the primary group at this time, the side where Q_{31} and Q_{32} are located can be defined as the primary side. Correspondingly, the side where Q_{43} and Q_{44} are located is the secondary side. At this time, the driving waveform of the bidirectional switch corresponding to the primary side and the secondary side is shown in Figure 17, The primary side bidirectional switch is composed of Q_{31} and Q_{32} in Figure 16, and the secondary side switch is composed of Q_{43} and Q_{44}, and the corresponding voltage and current waveforms of bidirectional switch are shown in Figure 18. The battery group SOC change curve during the equalization process is shown in Figure 19. After balancing, the voltages of G_1, G_2, G_3, and G_4 are set to 14.213 V, 14.243 V, 14.251 V and 14.260 V, respectively. The entire process takes 877.8 s. The equalization efficiency can be calculated according to Equation (23).

$$\eta = \frac{P_o}{P_{in}} = \frac{U_{2ndrms} I_{2ndrms}}{U_{1strms} I_{1strms}} \tag{23}$$

U_{1strms} is the effective value of the voltage on the primary side, and I_{1strms} is the effective value of the current on the primary side. U_{2strms} is the effective value of the voltage on the secondary side, and I_{2strms} is the effective value of the current on the secondary side. The above four quantities are calculated as Equation (24).

$$\begin{aligned} U_{1strms} &= \sqrt{\frac{1}{T}\int_0^T u_{1st}^2(t)dt} \\ I_{1strms} &= \sqrt{\frac{1}{T}\int_0^T i_{1st}^2(t)dt} \\ U_{2ndrms} &= \sqrt{\frac{1}{T}\int_0^T u_{2nd}^2(t)dt} \\ I_{2ndrms} &= \sqrt{\frac{1}{T}\int_0^T i_{2nd}^2(t)dt} \end{aligned} \tag{24}$$

After calculation, the equilibrium efficiency is $\eta \approx 87.3\%$.

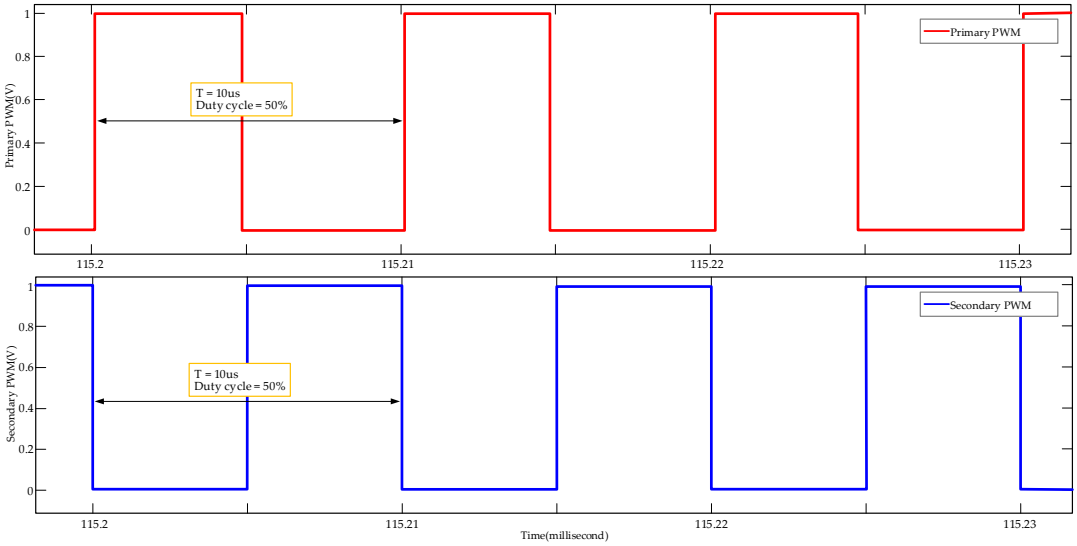

Figure 17. Driving waveform of the bidirectional switch.

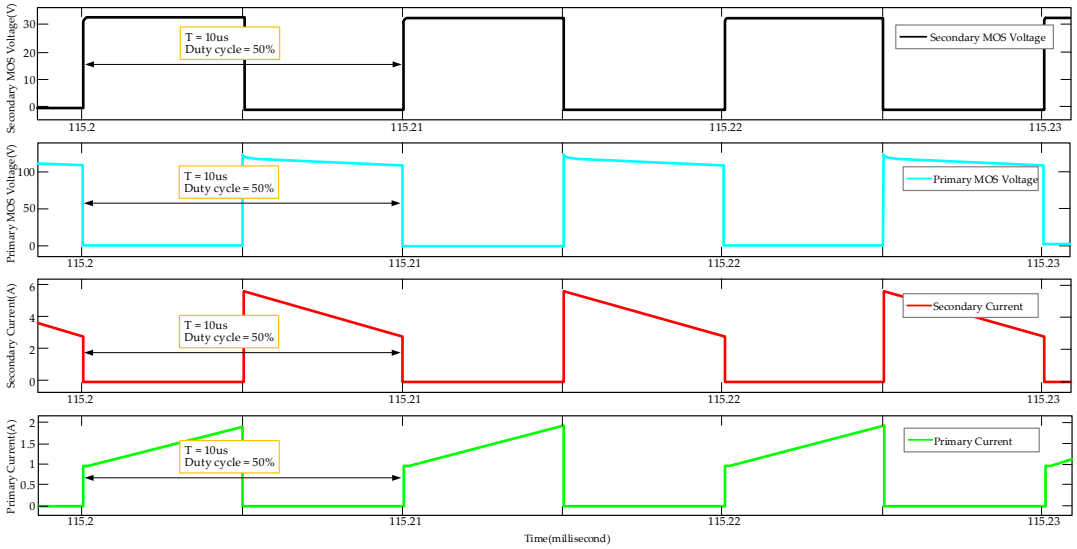

Figure 18. Voltage and current waveforms of the bidirectional switch.

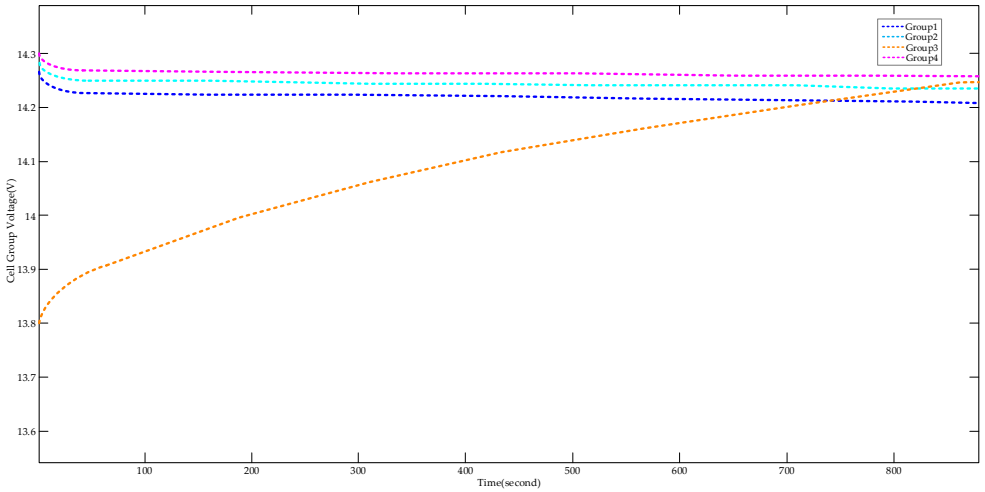

Figure 19. The SOC curve of CASE 1 during balancing in MODE 4.

(b) CASE 2: One battery group charges the entire power supply system.

In the power supply system, the initial voltages of G_1, G_2, G_3, and G_4 are set to 14.253 V, 14.275 V, 15.191 V, and 14.287 V, respectively. At this time, the battery group G_3 with the highest voltage should be used to charge the entire power supply system. Q_{31}, Q_{32}, Q_{43}, and Q_{44} shown in Figure 20 are controlled by two complementary PWMs, respectively. Since the entire power supply system is charged for the battery group at this time, Q_{31} and Q_{32} are located in the primary side, and Q_{44} is on the secondary side. At this time, the driving voltage waveforms of the primary side and secondary side MOS driving voltages are shown in Figure 20, and the voltage and current waveforms are shown in Figure 21. The battery group voltage change curve is shown in Figure 22. After the balancing is completed, the voltages of G_1, G_2, G_3, and G_4 are 14.260 V, 14.284 V, 14.262 V, and 14.293 V, respectively. The entire process takes 803.8 s. According to Equations (20) and (21), the equilibrium efficiency is $\eta \approx 83.4\%$.

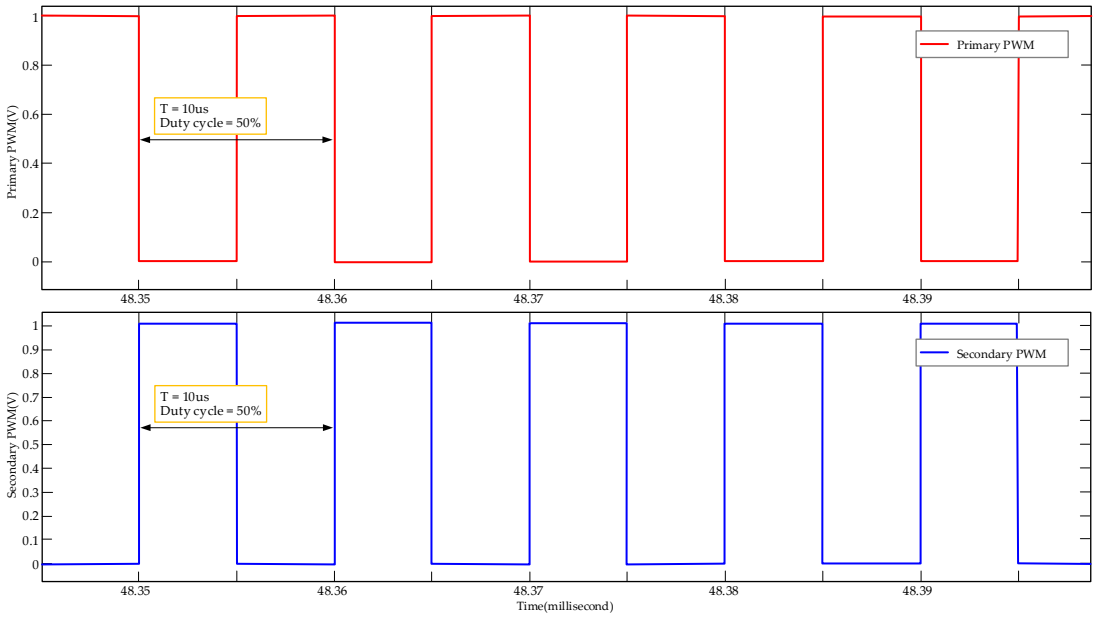

Figure 20. Driving waveform of the bidirectional switch.

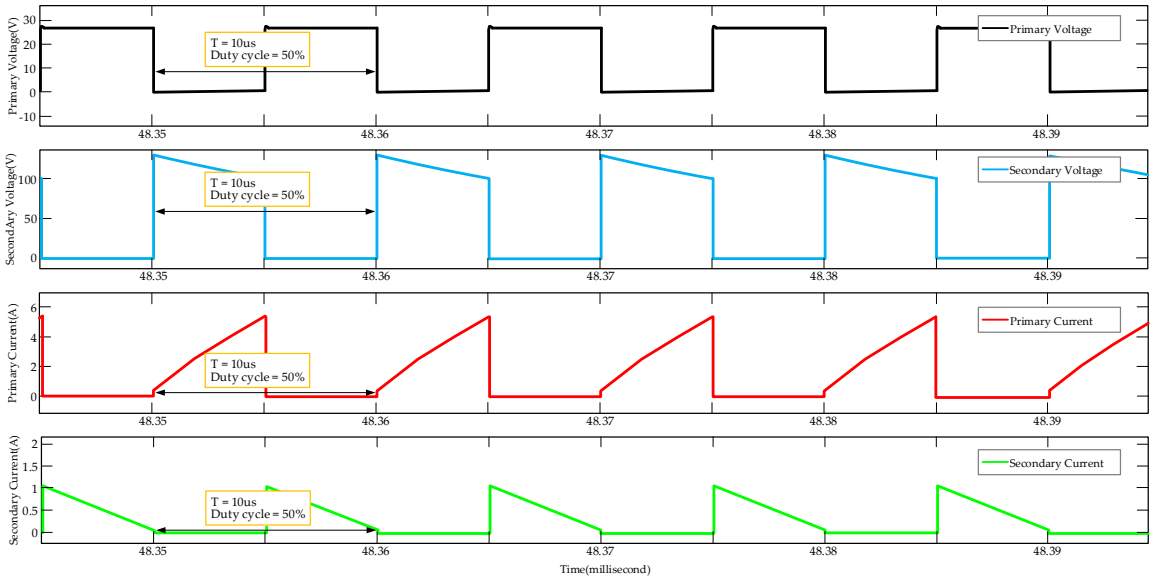

Figure 21. Voltage and current waveforms of the bidirectional switch.

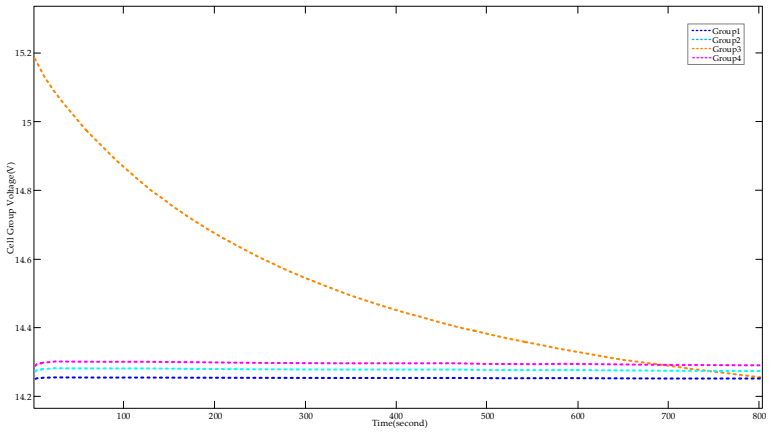

Figure 22. The SOC curve of CASE 2 during balancing in MODE 4.

4. Experimental Verification

In this section, the simulation verification of the entire battery equalization system is completed, which proved the feasibility of the scheme. Based on the scheme, we produced a physical circuit system. The transformer used is a planar transformer with a small volume, and the coil is made of a multilayer printed circuit board (PCB). The multilayer PCB increases the apparent power of the transformer. The actual battery balance system consists of three STM32 series microcontrollers as the control core, the microcontroller models are STM32F103C8T6, STM32F030C8T6, STM32F407ZET6, respectively. The three balancing control boards communicate with each other through the CAN bus version 2.0B. The feasibility of the scheme is further verified by the physical circuit system, the battery parameters, key switching devices and transformer parameters, which are listed in Tables 4 and 5, the calculation process of the theoretical value has been deduced in the previous chapter, so it is only listed here. The prototype is shown in Figure 23.

Table 4. Intra-group parameters.

Circuit Parameters	Description
Battery cell type	Ternary polymer lithium battery
Battery cell rated parameters	3.7 V/2.8 Ah
Switching frequency	100 kHz
Intra-group turn ratio	4:1
Intra-group transformer core	EE55
Duty cycle	45%
Intra-group topology power	40 W
Intra-group topology magnetizing inductance	73.7 uH
Intra-group topology leakage inductance	4.3 uH
Intra-group power switches	IRF640

Table 5. Inter-group parameters.

Circuit Parameters	Description
Switching frequency	100 kHz
Inter-group turn ratio	1:1:1:1
Inter-group Transformer core	EE32
Duty cycle	45%
Inter-group topology power	4.5 W
Inter-group topology magnetizing inductance	3.54 uH
Inter-group topology leakage inductance	0.24 uH
Inter-group power switches	DMN2300UFD

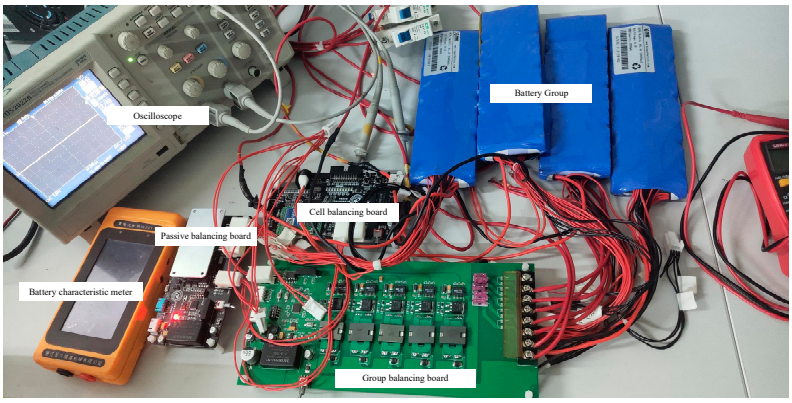

Figure 23. Overall effect diagram of the prototype.

As shown in Figure 24a–c, the experimental equilibrium data of MODE 1, MODE 2 and MODE 3 are obtained, which are basically consistent with the simulation results in Figures 11, 14 and 15, respectively. Experimental results show that the proposed hybrid equalization strategy is effective.

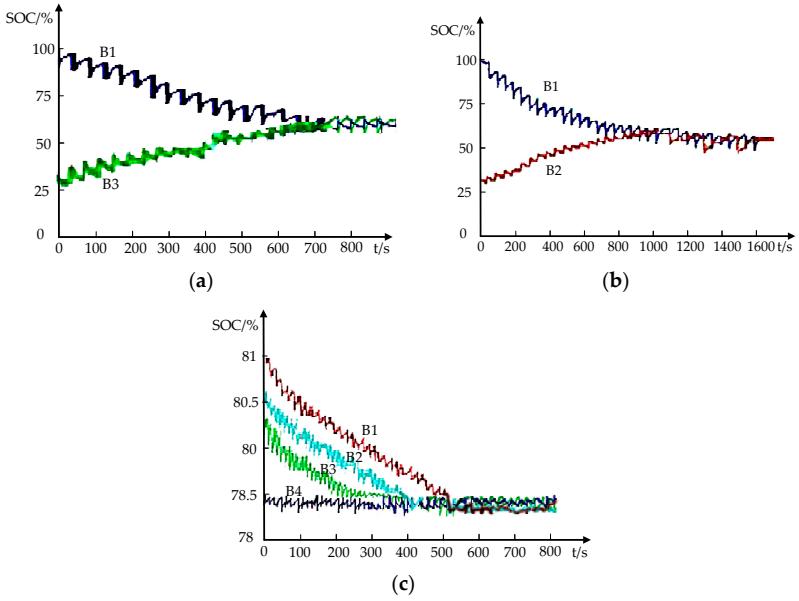

Figure 24. The SOC curve during balancing by experiments: (**a**) in MODE 1; (**b**) in MODE 2; and (**c**) in MODE 3.

As shown in Figure 25a,b, the experimental equilibrium data of CASE 1 and CASE 2 in MODE 4 are obtained, respectively, which are basically consistent with the simulation results in Figures 19 and 22, respectively. Experiments further verify the effectiveness of the proposed hybrid equalization strategy.

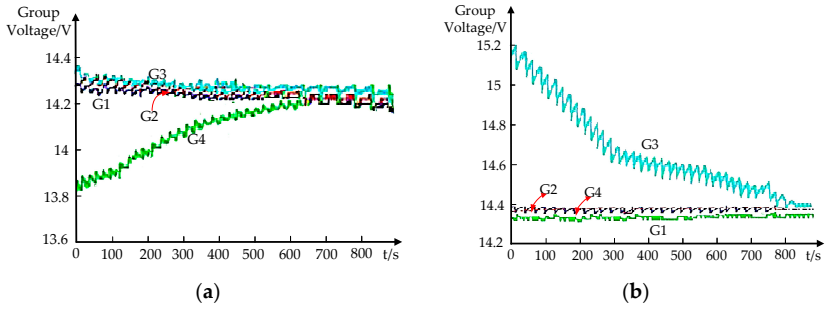

Figure 25. The SOC curve during balancing in MODE 4 by experiments: (**a**) CASE 1; and (**b**) CASE 2.

The following is an analysis of the balance process between the battery strings of other lengths. Taking a battery string composed of 20 cells as an example, the imbalance state is shown in Table 6.

Table 6. Battery imbalance condition.

Voltage(V)	Group	Cell1(V)	Cell2(V)	Cell3(V)	Cell4(V)
14.732	G_1	3.533	3.725	3.612	3.862
14.553	G_2	3.682	3.564	3.665	3.642
15.364	G_3	3.847	3.835	3.840	3.842
15.286	G_4	3.832	3.645	3.992	3.817
14.952	G_5	3.812	3.746	3.802	3.592

The unbalance conditions introduced above include unbalance within groups and unbalance between groups. The overall balance process is shown in Figure 26.

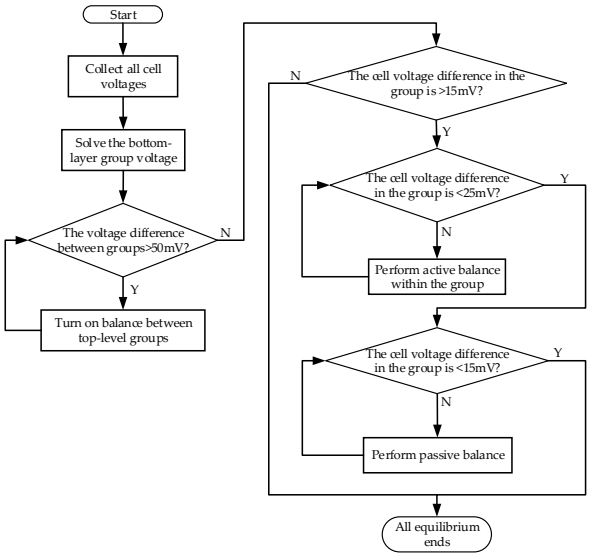

Figure 26. Long string battery pack balancing process.

According to the process shown in Figure 26 above, after the execution is completed, the gap between the batteries can be reduced to within the threshold range. This proves that the topology mentioned in the article has the ability to balance longer battery strings. As shown in Figure 27, different colors represent different battery packs; the batteries imbalance condition is shown in Table 6, according to the control strategy in this article, and this is the balancing process of five battery groups, a total of 20 battery cells.

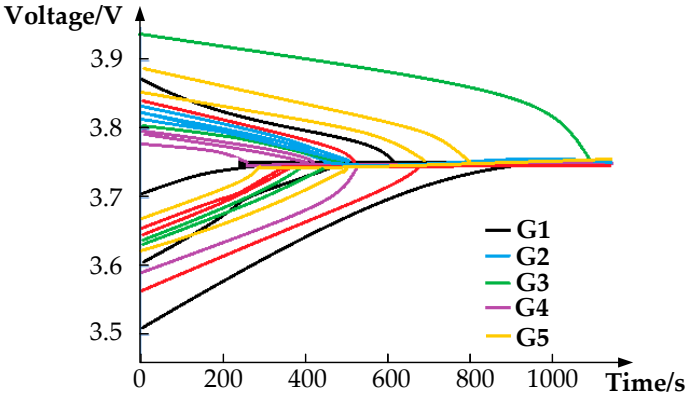

Figure 27. The balancing process of five battery groups.

5. Conclusions

In order to solve the problem of the inconsistent battery cell of the lithium battery group more effectively, this paper proposes a novel topology for hybrid lithium-ion battery cell balancing, and introduced the structure and working principle of the topology. We verify it by MATLAB 2018b /Simulink, and made an actual circuit system based on this topology. The experimental results show that the topology proposed in this paper has high equalization efficiency and fast equalization speed in the experiment. The experimental results confirm that the proposed hybrid equilibrium scheme has a certain improvement in the equilibrium speed compared with the full active equilibrium scheme. It used the passive equilibrium scheme to reduce the waiting time of the final stage of equilibrium, and it has a higher practical application value. The proposed topology achieved an excellent result, the proposed scheme has been verified by the simulation and experiment, but the top-layer equilibrium topology only realizes the energy exchange between the top-level group and any bottom-layer group, This topology can theoretically realize energy exchange between any bottom layer group, but more switches will pass through energy transmission, which leads to increased control logic complexity and switching loss will increase. This part of the function needs to be optimized in subsequent work.

Author Contributions: Conceptualization, M.G. and H.L. (Huipin Lin); methodology, H.L. (Huipin Lin). and Z.D.; software, Z.D.; validation, Z.D., J.Q. and H.L. (Hao Lan); formal analysis, J.Q.; investigation, H.L. (Huipin Lin); resources, M.G.; data curation, J.Q.; writing—original draft preparation, W.Z.; writing—review and editing, H.L. (Hao Lan); project administration, Q.W. and Z.D.; funding acquisition, M.G. All authors have read and agreed to the published version of the manuscript.

Funding: This research was funded by National Natural Science Foundation Project of China (grant number 61671194) and the Open Fund of Zhejiang Provincial Key Lab of Equipment Electronics (2019E10009).

Conflicts of Interest: The authors declare no conflict of interest.

References

1. Chen, Y.; Liu, X.; Cui, Y.; Zou, J. MultiWinding Transformer Cell-to-Cell Active Equalization Method for Lithium-Ion Batteries with Reduced Number of Driving Circuits. *IEEE Trans. Power Electron.* **2016**, *7*, 4916–4929.
2. Gallardo-Lozano, J.; Romero-Cadaval, E.; Milanes-Montero, M.I.; Guerrero-Martinez, M.A. Battery equalization active methods. *J. Power Sources* **2014**, *246*, 934–949. [CrossRef]
3. Lu, L.; Han, X.; Li, J.; Hua, J.; Ouyang, M. A review on the key issues for lithium-ion battery management in electric vehicles. *J. Power Sources* **2013**, *226*, 272–288. [CrossRef]
4. Rahimi-Eichi, H.; Ojha, U.; Baronti, F.; Chow, M. Battery Management System: An Overview of Its Application in the Smart Grid and Electric Vehicles. *IEEE Ind. Electron. Mag.* **2013**, *7*, 4–16. [CrossRef]
5. Zhou, Z.; Shang, Y.; Duan, B.; Zhang, C. An Any-Cell(s)-to-Any-Cell(s) Equalizer Based on Bidirectional Inductor Converters for Series Connected Battery String. In Proceedings of the IEEE 11th Conference on Industrial Electronics and Applications (ICIEA), Hefei, China, 5–7 June 2016; pp. 2511–2515.
6. Li, S.; Mi, C.C.; Zhang, M. A High-Efficiency Active Battery-Balancing Circuit Using Multiwinding Transformer. *IEEE Trans. Ind. Appl.* **2013**, *49*, 198–207. [CrossRef]
7. Wang, S.; Kang, L.; Guo, X.; Wang, Z.; Liu, M. A Novel Layered Bidirectional Equalizer Based on a Buck-Boost Converter for Series-Connected Battery Strings. *Energies* **2017**, *10*, 1011. [CrossRef]
8. Shang, Y.; Xia, B.; Zhang, C.; Cui, N.; Yang, J.; Mi, C.C. An Automatic Equalizer Based on Forward–Flyback Converter for Series-Connected Battery Strings. *IEEE Trans. Ind. Electron.* **2017**, *64*, 5380–5391. [CrossRef]
9. Zhang, Z.; Gui, H.; Gu, D.; Yang, Y.; Ren, X. A Hierarchical Active Balancing Architecture for Lithium-Ion Batteries. *IEEE Trans. Power Electron.* **2017**, *32*, 2757–2768. [CrossRef]
10. Bouchhima, N.; Schnierle, M.; Schulte, S.; Birke, K.P. Active model-based balancing strategy for self-reconfigurable batteries. *J. Power Sources* **2016**, *322*, 129–137. [CrossRef]
11. Cao, X.; Zhong, Q.C.; Qiao, Y.C.; Deng, Z.Q. Multi-layer Modular Balancing Strategy for Individual Cells in a Battery Pack. *IEEE Trans. Energy Convers.* **2018**, *33*, 526–536. [CrossRef]
12. Yarlagadda, S.; Hartley, T.T.; Husain, I. A Battery Management System Using an Active Charge Equalization Technique Based on a DC/DC Converter Topology. *IEEE Trans. Ind. Appl.* **2013**, *49*, 2720–2729. [CrossRef]

13. Lee, K.M.; Lee, S.W.; Choi, Y.G.; Kang, B. Active Balancing of Li-Ion Battery Cells Using Transformer as Energy Carrier. *IEEE Trans. Ind. Electron.* **2017**, *64*, 1251–1257. [CrossRef]
14. Li, Y.; Han, Y. A Module-Integrated Distributed Battery Energy Storage and Management System. *IEEE Trans. Power Electron.* **2016**, *31*, 8260–8270. [CrossRef]
15. Lim, C.S.; Lee, K.J.; Ku, N.J.; Hyun, D.S.; Kim, R.Y. A Modularized Equalization Method Based on Magnetizing Energy for a Series-Connected Lithium-Ion Battery String. *IEEE Trans. Power Electron.* **2014**, *29*, 1791–1799. [CrossRef]
16. Qi, X.; Wang, Y.; Fang, M. An Integrated Cascade Structure-Based Isolated Bidirectional DC—DC Converter for Battery Charge Equalization. *IEEE Trans. Power Electron.* **2020**. [CrossRef]
17. Farzan Moghaddam, A.; Van den Bossche, A. An efficient equalizing method for lithium-ion batteries based on coupled inductor balancing. *Electronics* **2019**, *8*, 136. [CrossRef]
18. Chin, C.; Gao, Z.C. State-of-Charge Estimation of Battery Pack under Varying Ambient Temperature Using an Adaptive Sequential Extreme Learning Machine. *Energies* **2018**, *11*, 711. [CrossRef]
19. Gao, Z.C.; Chin, C.S.; Toh, W.D.; Chiew, J.; Jia, J. State-of-Charge Estimation and Active Cell Pack Balancing Design of Lithium Battery Power System for Smart Electric Vehicle. *J. Adv. Transp.* **2017**, *2*, 1–14. [CrossRef]
20. Gao, Z.C.; Chin, C.; Chiew, J.; Jia, J.B.; Zhang, C.Z. Design and Implementation of Smart Lithium-ion Battery System with Real-time Fault Diagnosis Capability for Electric Vehicles. *Energies* **2017**, *10*, 1503. [CrossRef]
21. Gao, Z.C.; Chin, C.; Woo, W.; Jia, J.B. Integrated Equivalent Circuit and Thermal Model for Simulation of Temperature-Dependent LiFePO4 Battery in Actual Embedded Application. *Energ. Spec. Issue Control. Energy Storage* **2017**, *10*, 85. [CrossRef]
22. Wang, L.; Feng, B.; Wang, B.; Wu, T.; Lin, H. Bidirectional Short-Circuit Current Blocker for DC Microgrid Based on Solid-State Circuit Breaker. *Electronics* **2020**, *9*, 306. [CrossRef]